

# Topology Preserving Relaxation Labeling for Nonrigid Point Matching

Jong-Ha Lee, *Student Member, IEEE*, and  
Chang-Hee Won, *Member, IEEE*

**Abstract**—This paper presents a relaxation labeling process with the newly defined compatibility measure for solving a general nonrigid point matching problem. In the literature, there exists a point matching method using relaxation labeling; however, the compatibility coefficient takes a binary value of zero or one depending on whether a point and a neighbor have corresponding points. Our approach generalizes this relaxation labeling method. The compatibility coefficient takes  $n$  discrete values which measure the correlation between point pairs. In order to improve the speed of the algorithm, we use a diagram of log distance and polar angle bins to compute the correlation. The extensive experiments show that the proposed topology preserving relaxation algorithm significantly improves the matching performance compared to other state-of-the-art point matching algorithms.

**Index Terms**—Point pattern matching, graph matching, registration, relaxation labeling, nonrigid point matching.

## 1 INTRODUCTION

POINT matching is widely used in computer vision and pattern recognition because point representations are generally easy to extract [1], [2]. The point matching problem can be categorized as rigid matching and nonrigid matching based on the deformation of objects captured in the images [3]. Compared with a rigid case, a nonrigid matching is more complex. Most nonrigid point matching methods use an iterated estimation framework to find appropriate correspondence and transformation [4]. The iterated closest point (ICP) algorithm is one of the most well-known heuristic approaches [5]. It utilizes the relationship by assigning the correspondence with binary values of zero or one. However, in the case of nonrigid transformation, this binary assumption is no longer valid, especially when the deformation is large. The thin plate spline robust point matching (TPS-RPM) algorithm is a general framework to jointly solve for the feature correspondence as well as the geometric transformation [6]. The cost function that is being minimized is the sum of euclidean distances between the matching points. In TPS-RPM, the binary correspondence value of ICP is relaxed to the continuous value between zero and one. This soft-assign method improves the matching performance as the correspondences are able to improve gradually and continuously, without jumping around in the space of binary permutation matrices [7]. The algorithm is robust compared to ICP in the nonrigid case, but the joint estimation of correspondence and transformation increases the algorithm complexity. Furthermore, the euclidean distance makes sense only when there are at least rough initial alignments of the shapes. If the initial points are not aligned well, the matching result is poor. The coherent point drift (CPD) method is another probabilistic algorithm applied to the nonrigid point matching problem [8]. The CPD algorithm utilizes

the displacement field between two point sets and it has been extended to the general nonrigid registration framework with TPS-RPM as a special case [8]. Another approach is the shape context (SC) method, which uses an object recognizer based on the shape [9]. For each point, the distributions of the distance and orientation to the neighboring points are estimated through a histogram. There, distributions are used as the attribute relations for the points. The correspondences are decided by comparing each point's attributes in one set with the attributes of the other. Only the attributes are compared; thus, a search for the correspondences can be conducted more easily compared to ICP and TPS-RPM. Generally speaking, the SC method performs better in the handling of complex patterns than TPS-RPM. A recently proposed matching method, the robust point matching-preserving local neighborhood structures (RPM-LNS) algorithm, employs the notion of a neighborhood structure for the general point matching problem [10]. In RPM-LNS, the cost function is formulated as an optimization problem to preserve local neighborhood relations. The matching probability is refined through the relaxation labeling process. We will compare the performance of these algorithms with our approach.

Another interesting point matching approach is the kernel correlation (KC) based method [11]. The cost function of KC is proportional to the correlation of two kernel density estimates. The work was extended by using the L2 distance between Gaussian mixture models representing the point set [12]. Since the root-mean-square (RMS) matching errors of the KC approach and the L2 distance approach are relatively higher than the other available algorithms such as TPS-RPM, SC, RPM-LNS, and CPD, we have not included the matching results of these two methods in the experimental results.

In this paper, we generalize RPM-LNS by introducing the optimal compatibility coefficient for the relaxation labeling method to solve a nonrigid point matching problem. The relaxation labeling is an iterative procedure that reduces local ambiguities and achieves global consistency by exploiting contextual information which is quantitatively represented by "compatibility coefficient" [13], [14]. The theoretical grounds for standard relaxation labeling processes are found in [22]. The theory of probabilistic relaxation for matching features extracted from 2D images has been examined in [23]. It is widely known that the relaxation labeling process is greatly affected by the choice of the compatibility coefficient [15], [16]. The compatibility coefficients required for performing graph matching by probabilistic relaxation have been determined in [24]. In the method of Zheng and Doermann, the compatibility coefficient value was a binary value of zero or one, depending on whether a point and its neighboring point have corresponding points [10]. In our method, the correlation between point pairs is measured by the proposed compatibility function, which quantifies the amount of similarity and spatial smoothness between the point pairs in  $n$ -discrete values. This contextual information combined with a relaxation labeling process is used to search for a correspondence. Then the transformation is calculated by the thin plate spline (TPS) model [17]. These two processes are iterated until the optimal correspondence and transformation are found. The proposed relaxation labeling, with a new compatibility coefficient, preserves a topology of point set; thus, we call our method the topology preserving relaxation labeling (TPRL) algorithm. It is important to note that changing compatibility coefficient improves the matching performance significantly. In this paper, we compare the performance of TPRL with other algorithms.

The reminder of the paper is organized as follows. In Section 2, we review a point matching problem formulation as an optimization problem. In Section 3, we define new compatibility coefficient and present the relaxation labeling process in a point matching problem. We then show the robustness of our approach compared to the other algorithms in Section 4. Finally, we draw conclusions in Section 5.

• The authors are with the Department of Electrical and Computer Engineering, Temple University, 1947 N. 12th Street, Philadelphia, PA 19122. E-mail: {jong, cwon}@temple.edu.

Manuscript received 4 Mar. 2009; revised 3 Dec. 2009; accepted 10 Aug. 2010; published online 22 Sept. 2010.

Recommended for acceptance by M. Pelillo.

For information on obtaining reprints of this article, please send e-mail to: [tpami@computer.org](mailto:tpami@computer.org), and reference IEEECS Log Number TPAMI-2009-03-0145.

Digital Object Identifier no. 10.1109/TPAMI.2010.179.

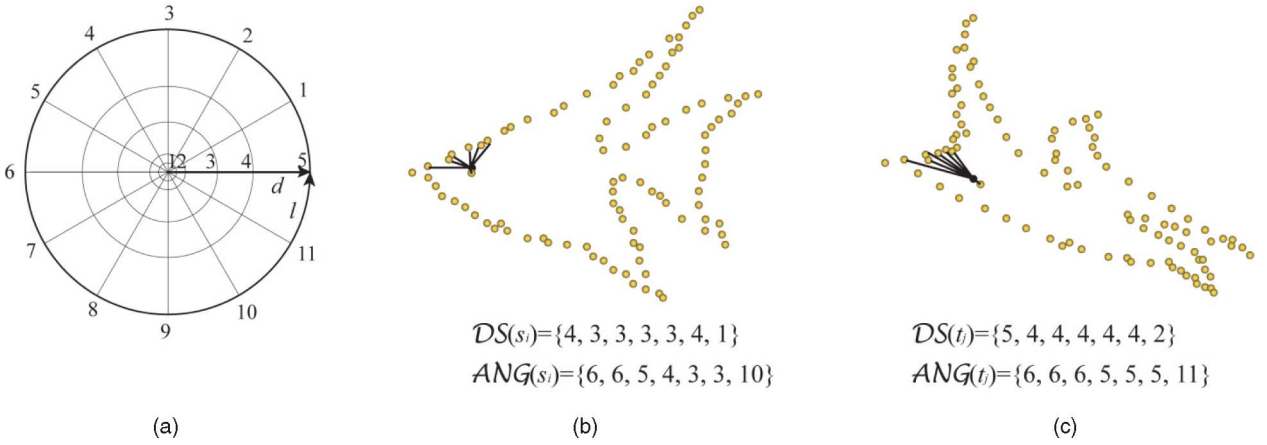


Fig. 1. The distance and angle computation. (a) Diagram of log-polar bins used in computing the distance and angle. We use five bins for the distances and 12 bins for the angles. (b) A point  $s_i \in S$  (black) from the fish shape with its sets  $DS(s_i)$  and  $ANG(s_i)$  of its six adjacent points in  $S$ . (c) The point  $t_j \in T$  (black) in the deformed fish shape which has six adjacent points and its distance and angle sets  $DS(t_j)$  and  $ANG(t_j)$ .

## 2 PROBLEM FORMULATION

Let  $s = \{s_1, s_2, \dots, s_I\}$  be a set of points in a model shape and  $T = \{t_1, t_2, \dots, t_J\}$  be a set of points in the target shape. Usually in a point matching problem, one-to-one matching is impossible because of the outliers. To handle this problem, we introduce dummy points,  $s_{nil}$  and  $t_{nil}$ , and then two point sets are augmented to  $S' = \{s_1, s_2, \dots, s_I, s_{nil}\}$  and  $T' = \{t_1, t_2, \dots, t_J, t_{nil}\}$ . The common points can be matched one-to-one and outliers can be matched to the dummy point. For a given point,  $s_i \in S'$ , one can select adjacent points  $a_x^{s_i}$ ,  $x = 1, \dots, X$ , which reside in the circle centered at  $s_i$ . We set the radius of a circle as the median value of all euclidean distances between point pairs in  $S$ . Similarly, for a point  $t_j \in T'$ , adjacent points are  $a_y^{t_j}$ ,  $y = 1, \dots, Y$ , and  $Y$  is the total number of adjacent points of  $t_j$ .

In this paper, the point matching problem is formulated as the graph matching problem. Each point is a node of a graph, and a point and its adjacent point constitute the edges of the graph. Then the problem is to maximize the number of matched edges between two graphs. For this purpose, we determine the fuzzy correspondence matrix  $P$ . Each entry of  $P$  has continuous value between  $[0, 1]$  that indicates the weight of the correspondence between  $s_i$  and  $t_j$ . The optimal match  $P$  is found by maximizing the energy function as follows:

$$\hat{P} = \arg \max_P C(S', T', P), \quad (1)$$

where  $C(S', T', P)$  is the energy function which is optimized by the probabilistic relaxation method [25].

## 3 POINT CORRESPONDENCE USING RELAXATION LABELING

Here, we use the relaxation labeling process to solve the optimization problem of nonrigid point matching. The relaxation labeling is an iterative process to reduce ambiguities in assigning labels to a set of objects by incorporating the contextual information. The contextual information is usually represented as the compatibility coefficient. In this paper, we propose a compatibility coefficient that suitably preserves the topology during the matching process.

### 3.1 Topology Preserving Relaxation Labeling with New Compatibility Coefficient

Initially, each point  $s_i \in S'$  is assigned a set of matching probability based on the shape context distance. After the initial probability assignment, the relaxation labeling process updates the matching probability. The purpose of the subsequent process is to assign a

matching probability that maximizes  $C(S', T', P)$  under the relaxed condition as  $P_{s_i t_j} \in [0, 1]$ . At the end of the relaxation labeling process, it is expected that each point will have one unambiguous matching probability. We follow the relaxation labeling updating rule of [18]: 1) Compute the compatibility coefficient which imposes the similarity and spatial smoothness constraints between point pairs. 2) Compute the support function from all compatibility coefficients related to the point. 3) Update the matching probability depending on its support function.

The determination of the compatibility coefficients is crucial because the performance of the relaxation labeling process depends on them. As a key contribution, we define a new compatibility coefficient to relax the binary value into multiple discrete values. The proposed compatibility coefficient quantifies the degree of agreement between the hypothesis that  $s_i$  matches to  $t_j$  and  $a_x^{s_i}$  matches to  $a_y^{t_j}$ . It is measured by the set of vectors originating from a point and extending to all other sample points. The full set of vectors increases the algorithm complexity and processing time. To simplify and speed up the process, log distance and polar angle bins are used to capture the coarse location information [9]. The bins are uniform in log-polar space, which makes the descriptor more sensitive to positions of adjacent points than to those of points far apart. In the diagram, the distance is defined as zero in the origin and incremented by one toward the outer bins, as shown in Fig. 1a. More specifically, the bin distance measure quantifies the original euclidean distance from 0 to 5, where 0 indicates the shortest euclidean distance and 5 indicates the longest euclidean distance. The euclidean distance uses multiple digits. Because we use only one digit to represent the distance, the computational complexity of the distance measure is reduced compared to the arbitrary euclidean distance measure. Let  $d_i(s_i, a_x^{s_i}) \in \mathbb{N}$  be the distance between origin point  $s_i$  and its nearest adjacent points. Then the distance set of an origin point  $s_i$  is defined as  $DS(s_i) = \{d(s_i, a_1^{s_i}), d(s_i, a_2^{s_i}), \dots, d(s_i, a_X^{s_i})\}$ . For the computation of the angle between point pairs, the alignment of a diagram with a reference point is necessary. In this paper, the mass center of a point set is used as a reference point. The direction from a point to the center of mass is set as the positive x-axis of the descriptor. From this axis, the angle is incremented by 1 in a counterclockwise direction. Let  $l_i(s_i, a_x^{s_i}) \in \mathbb{N}$  be the angle between origin point  $s_i$  and its nearest adjacent points. The angle set of an origin point  $s_i$  is given as  $ANG(s_i) = \{l_i(s_i, a_1^{s_i}), l_i(s_i, a_2^{s_i}), \dots, l_i(s_i, a_X^{s_i})\}$ . Every point can be an origin and the origin varies with points in consideration to calculate the location information. Figs. 1b and 1c show the distance and angle sets for a given point  $s_i \in S$  and its corresponding point  $t_j \in T$ .

In the nonrigid degradation of point sets, we note that a point set is usually distorted; however, the neighboring structure of a point is generally preserved due to physical constraints. The displacement of a point and its adjacent point between two point sets constrains one another. Thus, if the distance and angle of a point pair  $(s_i, a_x^{s_i})$  in the model shape and its corresponding point pair  $(t_j, a_y^{t_j})$  in the target shape are similar, we say that they have high correlation. This is further strengthened if a point pair  $(s_i, a_x^{s_i})$  in the model shape is closer to each other. To quantify this knowledge, we introduce the similarity constraint,  $\alpha, \beta$ , as well as the spatial smoothness constraint,  $\gamma$ .

The first constraint is the similarity which is related to the differences between the distances and angles of  $(s_i, a_x^{s_i})$  and  $(t_j, a_y^{t_j})$ . This first constraint imposes that if  $(s_i, a_x^{s_i})$  has smaller distance and angle differences with  $(t_j, a_y^{t_j})$ , then they are more compatible. The disparities between  $(s_i, a_x^{s_i})$  and  $(t_j, a_y^{t_j})$  are defined as follows:

$$\alpha(s_i, a_x^{s_i}; t_j, a_y^{t_j}) = \left(1 - \left| \frac{d_i(s_i, a_x^{s_i}) - d_j(t_j, a_y^{t_j})}{\max_{m,n} \{d_m(s_m, a_x^{s_m}), d_n(t_n, a_y^{t_n})\}} \right| \right), \quad (2)$$

$$\beta(s_i, a_x^{s_i}; t_j, a_y^{t_j}) = \left(1 - \left| \frac{l_i(s_i, a_x^{s_i}) - l_j(t_j, a_y^{t_j})}{\max_{m,n} \{l_m(s_m, a_x^{s_m}), l_n(t_n, a_y^{t_n})\}} \right| \right). \quad (3)$$

The second constraint, spatial smoothness, is measured by the distance between  $s_i$  and  $a_x^{s_i}$ :

$$\gamma(s_i, a_x^{s_i}) = \left(1 - d(s_i, a_x^{s_i}) / \max_m \{d_m(s_m, a_x^{s_m})\}\right), \quad (4)$$

where  $\max_m \{d_m(s_m, a_x^{s_m})\}$  is the longest edge of point-adjacent point pairs. Two points  $s_i$  and  $a_x^{s_i}$  are the most salient if  $\gamma(s_i, a_x^{s_i})$  is 1 and the least salient if  $\gamma(s_i, a_x^{s_i})$  is 0. The constraining relations are illustrated in Fig. 2.

We define a total compatibility coefficient by

$$r_{s_i t_j}(a_x^{s_i} a_y^{t_j}) = \alpha(s_i, a_x^{s_i}; t_j, a_y^{t_j}) \cdot \beta(s_i, a_x^{s_i}; t_j, a_y^{t_j}) \cdot \gamma(s_i, a_x^{s_i}). \quad (5)$$

Clearly,  $r_{s_i t_j}(a_x^{s_i} a_y^{t_j})$  ranges from 0 to 1. A high value of  $r_{s_i t_j}(a_x^{s_i} a_y^{t_j})$  corresponds to a high matching probability between  $(s_i, a_x^{s_i})$  and  $(t_j, a_y^{t_j})$ , and a low value corresponds to incompatibility. The support function  $q_{s_i t_j}^k$  in the  $k$ th iteration is given by

$$\begin{aligned} q_{s_i t_j}^k &= \sum_{i=1}^I \sum_{j=1}^J r_{s_i t_j}(a_x^{s_i} a_y^{t_j}) p_{a_x^{s_i} a_y^{t_j}}^k \\ &= \sum_{i=1}^I \sum_{j=1}^J \alpha(s_i, a_x^{s_i}; t_j, a_y^{t_j}) \cdot \beta(s_i, a_x^{s_i}; t_j, a_y^{t_j}) \cdot \gamma(s_i, a_x^{s_i}) p_{a_x^{s_i} a_y^{t_j}}^k. \end{aligned} \quad (6)$$

Note that  $r_{s_i t_j}(a_x^{s_i} a_y^{t_j})$  is weighted by  $p_{a_x^{s_i} a_y^{t_j}}^k$  because it depends on the likelihood of adjacent point pairs matching probability. Finally,  $p_{s_i t_j}^k$  is updated according to

$$p_{s_i t_j}^{k+1} = p_{s_i t_j}^k q_{s_i t_j}^k / \sum_{j=1}^J p_{s_i a_i^j}^k q_{s_i a_i^j}^k. \quad (7)$$

The optimization process is as follows: If a matching probability between  $s_i$  and  $t_j$  is supported from their adjacent points  $a_x^{s_i}$  and  $a_y^{t_j}$ , then the probability of being matched increases. The probability decreases if they have relatively small support from their adjacent points.

Traditionally, sum of rows (or columns) in the matrix  $p$  is used as a constraint in the relaxation labeling process. In this paper, we use sum of rows and columns as a two-way constraints. In order to meet these constraints, alternated row and column normalization of the matrix  $P$  is performed after each relaxation labeling updates. This

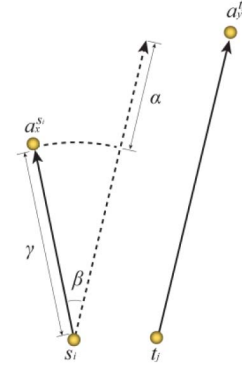


Fig. 2. The general case of the correlation strength depends on the differences of distance and angle between point pairs. The similarity constraints  $\alpha, \beta$  and the spatial smoothness constraint  $\gamma$  comprise the final compatibility coefficient for the relaxation labeling process.

procedure is known as Sinkhorn normalization and it showed that the procedure always converges to a doubly stochastic matrix [19].

After a predefined relaxation labeling iteration, the estimated matching probability is assigned to every point. To handle outliers, the points with the maximum matching probability less than a certain minimum probability (in our case, we set this to be  $P_{\min} = 0.95$ ) are labeled as outliers by matching them to a dummy point. The outlier rejection scheme is performed throughout the relaxation labeling process.

### 3.2 Transformation Model

The strategy of iterated point correspondence and transformation estimations for the best matching results is widely used for the nonrigid point matching [6]. This framework is followed in this paper. For the coordinate transformation, the TPS model is used. Suppose point  $(x_i, y_i)$  is matched to  $(u_i, v_i)$  for  $i = 1, 2, \dots, n$ . Let  $z_i = f(x_i, y_i)$  be the transformation function value at corresponding locations  $(x_i, y_i)$ . The TPS interpolant  $f(x, y)$  minimizes the bending energy  $I(f) = \int \int_{\mathbb{R}^2} (\partial^2 f / \partial x^2)^2 + 2(\partial^2 f / \partial x \partial y)^2 + (\partial^2 f / \partial y^2)^2 dx dy$  and has a solution of the form  $f(x, y) = a_1 + a_x x + a_y y + \sum_{i=1}^n w_i U(\|(x_i, y_i) - (x, y)\|)$  where  $U(r)$  is the kernel function, taking the form of  $U(r) = r^2 \log r^2$  and  $U(0) = 0$  [9]. Sometimes it is necessary to relax the exact interpolation by means of regularization. This is accomplished by minimizing the bending energy  $H[f] = \sum_{i=1}^n (z_i - f(x_i, y_i))^2 + \lambda I_f$ , where  $\lambda$  is the regularization parameter.

After several relaxation labeling updates, the parameters of the TPS deformation model are estimated from the matched point pairs. The estimated parameters are then used to transform the model set bringing it as close as possible to the target set. The relaxation labeling process then starts again between the transformed model set and the target set. The processes for identifying correspondence and transformation are alternatively iterated until the stopping criterion is met.

## 4 VALIDATION, COMPARATIVE ANALYSIS, AND PERFORMANCE EVALUATION

In order to access the performance of the proposed algorithm, we have compared our matching results with the state-of-the-art algorithms such as SC, TPS-RPM, RPM-LNS, and CPD method. In the experiments, we set 300 as the number of labeling updates and the alternate iteration with TPS transformation as 10.

### 4.1 Experiments Based on Synthetic Data

We have tested our proposed method and the state-of-the-art algorithms with respect to different degrees of deformation, noise,

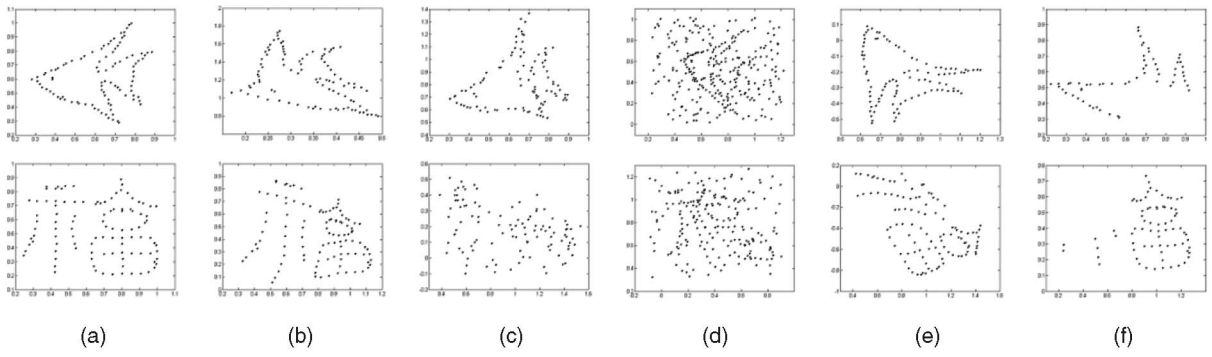


Fig. 3. Synthesized data sets for statistical tests. Model sets are shown in (a). Columns 2-6 show the target sets for the (b) deformation, (c) noise, (d) outlier, (e) rotation, and (f) occlusion.

outliers, rotation, and occlusion ratio on synthetic data set. The data set consists of two different shape models. The first model consists of 96 points to represent a fish shape. The second model is a more complex pattern consisting of 108 points to represent a Chinese character (“blessing”).

In each test, one of the distortions is applied to a model set to create a target set. Fig. 3 shows examples of synthesized data sets [6], [10]. A total of 100 data sets are generated at each distortion level. The matching performance of each algorithm is compared by the mean and standard deviation of the registration error of 100 trials in each distortion level. We use RMS error for the

registration error metric [20]. The statistical results, error means, and standard deviations for each setting are shown in Fig. 4.

In the deformation test results, Fig. 4a, five algorithms achieve similar matching performance in both fish and character shape at low deformation ratio. However, as the degree of deformation increases, we observe that TPRL shows the robustness to large deformation compared with other algorithms.

The presence of noise makes the point’s location ambiguous. Therefore, these types of data are more challenging than the deformation data. The noise test results of Fig. 4b show that all algorithms are affected by this type of data distortion. However,

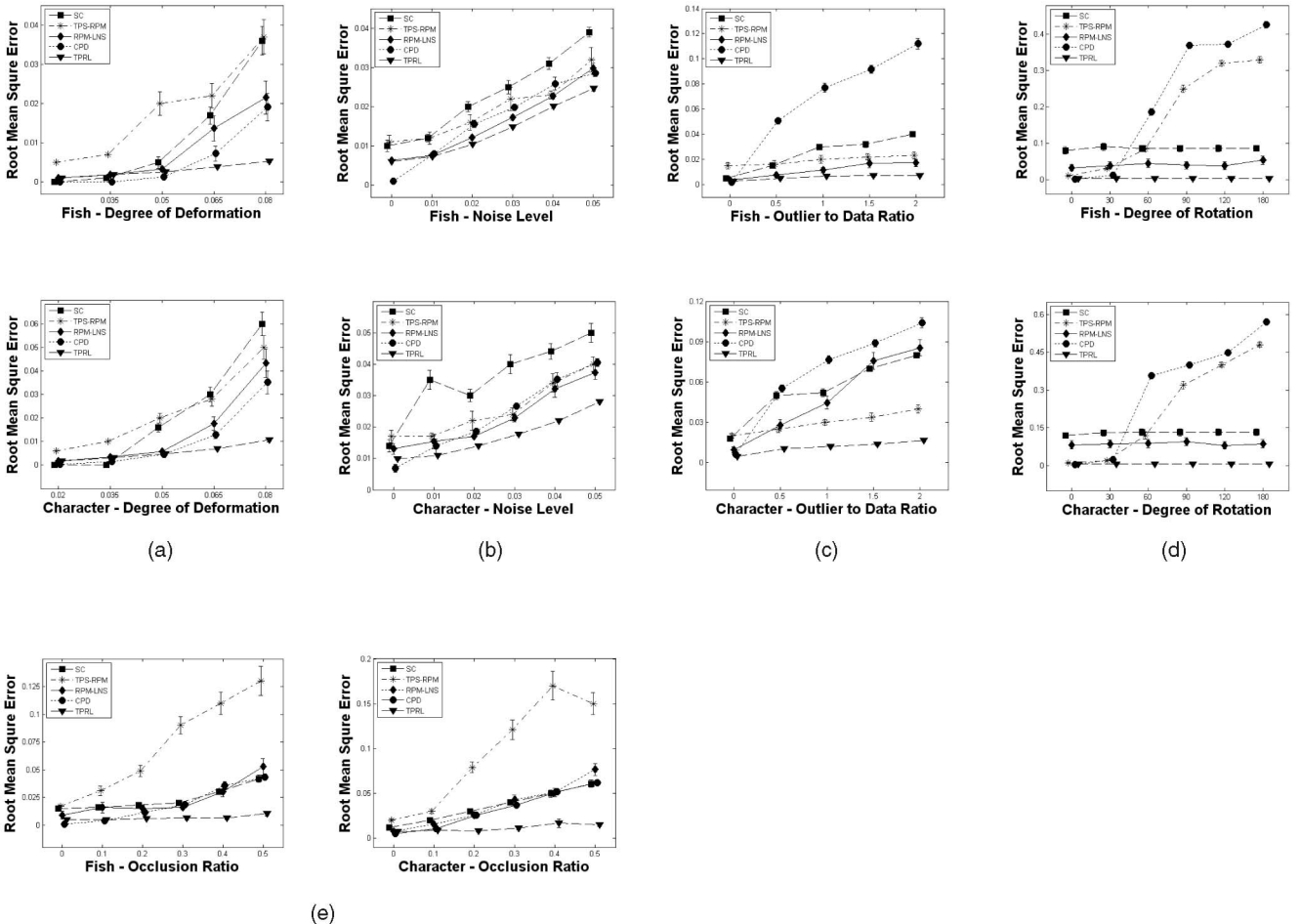


Fig. 4. Comparison of the matching performance of TPRL (▽) with shape context (□), TPS-RPM (\*), RPM-LNS (◊), and CPD (O) for the fish and character shapes. The error bars indicate the standard error of the mean over 100 trials. The results show that for the degradation of most data sets, the TPRL algorithm is more robust than the SC, TPS-RPM, RPM-LNS, and CPD methods. (a) Deformation test, (b) noise test, (c) outlier test, (d) rotation test, and (e) occlusion test.



Fig. 5. Sequence images of the toy hotel. Frames 0, 10, 20, 30, 40, 50, 60, 70, 80, 90, and 100.

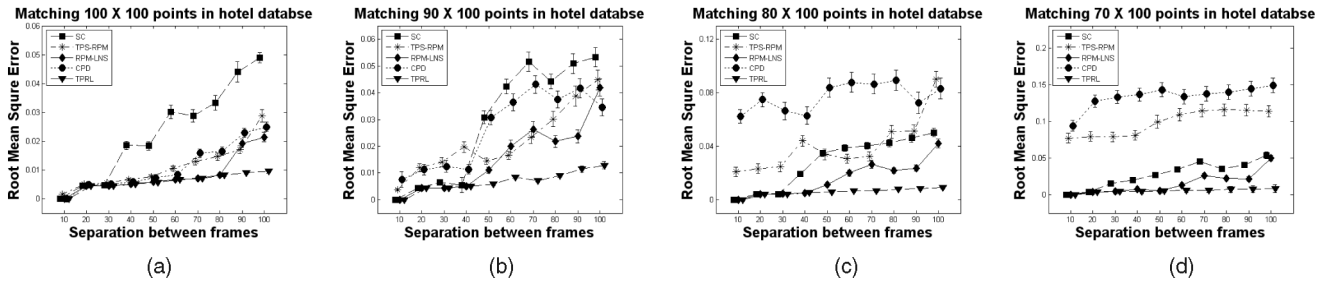


Fig. 6. Comparison of the matching performance of TPRL ( $\nabla$ ) with shape context ( $\square$ ), TPS-RPM ( $*$ ), RPM-LNS ( $\diamond$ ), and CPD ( $\circ$ ) in the hotel sequence for increasing frame separation and different occlusion ratios: (a) 0.0, (b) 0.1, (c) 0.2, (d) 0.3. Error bars correspond to the standard error of the mean of each pair's RMS error.

we notice that TPRL compensates for the location ambiguity and finds more accurate correspondences than the other four.

In addition to the deformation and noise test, present outliers further complicate the point matching problem. To evaluate the performance of our method with outliers, we added maximum of 405 outliers to the target set. From the results of Fig. 4c, we note that SC and CPD in both shapes and RPM-LNS in a character shape are easily confused by outliers and start to fail once the outlier level becomes relatively high. TPS-RPM is not affected by outliers as much, but the error is still higher than TPRL. TPRL is very robust, regardless of the outlier level.

In Fig. 4d, we evaluate the influence of rotation. From this result, we notice that the applied transformation (rotation) does not affect the performance of SC, RPM-LNS, and TPRL. All error curves except TPS-RPM and CPD are relatively constant. Note that until 30 degrees of rotation, the errors of TPS-RPM and CPD are lower than SC and RPM-LNS. But, from 60 degrees of rotation, TPS-RPM and CPD deteriorate quickly. TPRL is rotation invariant and consistently outperforms four other algorithms in all degrees of rotations.

Occlusion is also an important degradation in real applications. We use six occlusion levels to test the five algorithms. As shown in Fig. 4e, the RMS error of TPS-RPM is the largest compared to the other four algorithms. TPRL achieves the best result in both fish and character shapes.

## 4.2 Experiments Based on Real-World Data

We also conducted experiments on real-world data. For this experiment, we have used the CMU hotel sequence available at <http://vasc.ri.cmu.edu/idb/html/motion/hotel/>. The database consists of 101 frames of a moving sequence of a toy hotel. We obtained 11 frames as shown in Fig. 5. In total, 100 points were

manually selected from each frame and matched all images spaced by 10, 20, 30, 40, 50, 60, 70, 80, 90, 100 frames. The experiments were conducted under four different occlusion ratios: 0.0( $100 \times 100$ ), 0.1( $90 \times 100$ ), 0.2( $80 \times 100$ ), and 0.3( $70 \times 100$ ).

Fig. 6 shows the results for these experiments. We note that, without occlusion, Fig. 6a, five algorithms achieve similar matching performance until 30 frames of separation. However, as the frame separation increases, we observe that TPRL shows robustness compared to other algorithms. The increased mean RMS error from 10 to 100 frames of separation is 0.001 mm, compared to 0.049 mm in SC, 0.027 mm in TPS-RPM, 0.021 mm in RPM-LNS, and 0.025 mm in CPD. Figs. 6b, 6c, and 6d show the results with occlusion. With 0.3 occlusion ratio, the increased mean RMS error is 0.005 mm from 10 to 100 frames of separation, compared to 0.05 mm in RPM-LNS, the second smallest change among the algorithms.

## 4.3 Experiments Based on Large Data

We also tested the TPRL performance under a larger data set. The image in Fig. 7 is a straw image available at <http://sipi.usc.edu/database/>. From the image, 1,000 points were extracted by the curvature scale space corner detector [21]. After a model set was chosen, we applied a randomly generated nonrigid transformation to warp it and added 1,000 to 3,000 outliers. The TPRL performed the best with  $0.35 \pm 0.22$  mm,  $0.38 \pm 0.24$  mm, and  $0.39 \pm 0.25$  mm RMS errors for the  $1,000 \times 2,000$ ,  $1,000 \times 3,000$ , and  $1,000 \times 4,000$  size point matching, respectively. The CPD method gave the second highest matching performance with  $0.61 \pm 0.51$  mm,  $0.66 \pm 0.56$  mm, and  $0.67 \pm 0.56$  mm RMS errors in the same scenario.

## 4.4 Processing Times

In order to compare algorithms, it is necessary to analyze the processing time of each algorithm. Assume that both model set and target set have  $N$  points. The algorithms are based on the NP-hard problem and have similar computational complexity of  $O(N^2)$  for matching in  $\mathbb{R}^2$ . Among the compared algorithms, the CPD method performs with the fastest registration time under a large distortion of the data set. The TPRL algorithm takes a slightly longer time to compute compared to the CPD method. For a  $105 \times 105$  point matching, the TPRL algorithm takes about 1.69 s and the CPD method takes about 1.08 s on a desktop PC with Core 2 Duo CPU with 2.13 GHz and 2GB RAM.

## 5 CONCLUSIONS

In this paper, we presented a novel approach to the nonrigid point matching problem using a relaxation labeling process and newly

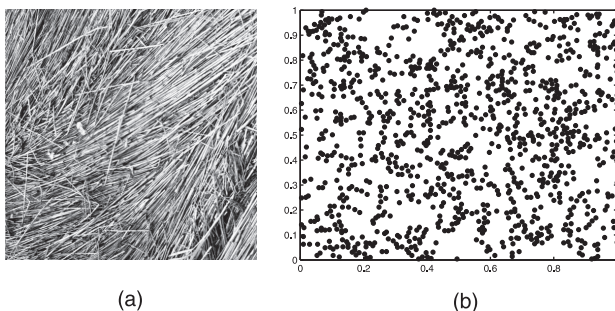


Fig. 7. Robustness test on a large data set. (a) A straw image and (b) 1,000 points extracted from the straw image.

defined compatibility function. The matching probability was updated by the relaxation process, taking into account the proposed compatibility. A comparative analysis has been performed against other state-of-the-art algorithms. The TPRL algorithm showed superior performance with both synthetic and real-world data.

## ACKNOWLEDGMENTS

The authors thank Dr. Haibin Ling for his helpful comments on the first draft of this document. This research is supported in part by the Tobacco Formula Fund from the Office of the Senior Vice Provost for Research and Strategic Initiatives at Temple University.

## REFERENCES

- [1] L.G. Brown, "A Survey of Image Registration Techniques," *ACM Computing Surveys*, vol. 24, no. 4, pp. 325-376, Dec. 1992.
- [2] H.J. Johnson and G.E. Christensen, "Consistent Landmark and Intensity-Based Image Registration," *IEEE Trans. Medical Imaging*, vol. 21, no. 5, pp. 450-461, May 2002.
- [3] B. Zitova and J. Flusser, "Image Registration Methods: A Survey," *Image and Vision Computing*, vol. 21, no. 11, pp. 977-1000, 2003.
- [4] A. Rangarajan, H. Chui, and F. Bookstein, "The Softassign Procrustes Matching Algorithm," *Medical Image Analysis*, vol. 4, pp. 1-17, 1999.
- [5] P.J. Besl and N.D. McKay, "A Method for Registration of 3D Shapes," *IEEE Trans. Pattern Analysis and Machine Intelligence*, vol. 14, no. 2, pp. 239-256, Feb. 1992.
- [6] H. Chui and A. Rangarajan, "A New Point Matching Algorithm for Nonrigid Registration," *Computer Vision and Image Understanding*, vol. 89, no. 23, pp. 114-141, 2003.
- [7] A. Rangarajan, S. Gold, and E. Mjolsness, "A Novel Optimizing Network Architecture with Applications," *Neural Computing*, vol. 8, no. 5, pp. 1041-1060, July 1996.
- [8] A. Myronenko, X. Song, and M.A. Carreira-Perpinan, "Nonrigid Point Registration: Coherent Point Drift," *Advances in Neural Information Processing Systems*, vol. 19, pp. 1009-1016, Springer, 2007.
- [9] S. Belongie, J. Malik, and J. Puzicha, "Shape Matching and Object Recognition Using Shape Contexts," *IEEE Trans. Pattern Analysis and Machine Intelligence*, vol. 24, no. 4, pp. 509-522, Apr. 2002.
- [10] Y. Zheng and D. Doermann, "Robust Point Matching for Nonrigid Shapes by Preserving Local Neighborhood Structures," *IEEE Trans. Pattern Analysis and Machine Intelligence*, vol. 28, no. 4, pp. 643-649, Apr. 2006.
- [11] Y. Tsin and T. Kanade, "A Correlation-Based Approach to Robust Point Set Registration," *Proc. Eighth European Conf. Computer Vision*, pp. 558-569, 2004.
- [12] B. Jian and B. Vemuri, "A Robust Algorithm for Point Set Registration Using Mixture of Gaussians," *Proc. 10th IEEE Int'l Conf. Computer Vision*, pp. 1246-1251, 2005.
- [13] A. Rosenfeld, R.A. Hummel, and S.W. Zucker, "Scene Labeling by Relaxation Operations," *IEEE Trans. System, Man, and Cybernetics*, vol. 6, no. 6, pp. 420-433, June 1976.
- [14] R.A. Hummel and S.W. Zucker, "On the Foundations of Relaxation Labeling Processes," *IEEE Trans. Pattern Analysis and Machine Intelligence*, vol. 5, no. 3, pp. 267-287, May 1983.
- [15] S. Peleg and A. Rosenfeld, "Determining Compatibility Coefficients for Curve Enhancement Relaxation Processes," *IEEE Trans. System, Man, and Cybernetics*, vol. 8, no. 7, pp. 548-555, July 1978.
- [16] M. Pelillo and M. Refice, "Learning Compatibility Coefficients for Relaxation Labeling Processes," *IEEE Trans. Pattern Analysis and Machine Intelligence*, vol. 16, no. 9, pp. 933-945, Sept. 1994.
- [17] F.L. Bookstein, "Principal Warps: Thin-Plate Splines and the Decomposition of Deformations," *IEEE Trans. Pattern Analysis and Machine Intelligence*, vol. 11, no. 6, pp. 567-585, June 1989.
- [18] Q.X. Wu and D. Pairman, "A Relaxation Labeling Technique for Computing Sea Surface Velocities from Sea Surface Temperature," *IEEE Trans. Geoscience and Remote Sensing*, vol. 33, no. 1, pp. 216-220, Jan. 1995.
- [19] R. Sinkhorn, "A Relationship between Arbitrary Positive Matrices and Doubly Stochastic Matrices," *The Annals of Math. Statistics*, vol. 35, no. 2, pp. 876-879, 1964.
- [20] K. Mikolajczyk and C. Schmid, "A Performance Evaluation of Local Descriptors," *IEEE Trans. Pattern Analysis and Machine Intelligence*, vol. 27, no. 10, pp. 1615-1630, Oct. 2005.
- [21] X.C. He and N.H.C. Yung, "Corner Detector Based on Global and Local Curvature Properties," *Optical Eng.*, vol. 47, no. 5, p. 057008, 2008.
- [22] M. Pelillo, "The Dynamics of Nonlinear Relaxation Labeling Processes," *J. Math. Imaging and Vision*, vol. 7, no. 4, pp. 309-323, Oct. 1997.
- [23] R.C. Wilson and E.R. Hancock, "A Bayesian Compatibility Model for Graph Matching," *Pattern Recognition Letters*, vol. 17, no. 3, pp. 263-276, Mar. 1996.
- [24] W. Christmas, J. Kittler, and M. Petrou, "Structural Matching in Computer Vision Using Probabilistic Relaxation," *IEEE Trans. Pattern Analysis and Machine Intelligence*, vol. 17, no. 8, pp. 749-764, Aug. 1995.

- [25] J. Kitter and E.R. Hancock, "Combining Evidence in Probabilistic Relaxation," *Int'l J. Pattern Recognition and Artificial Intelligence*, vol. 3, no. 1, pp. 25-51, Feb. 1989.

► For more information on this or any other computing topic, please visit our Digital Library at [www.computer.org/publications/dlib](http://www.computer.org/publications/dlib).